

In silico biomechanical design of the metal frame of transcatheter aortic valves: multi-objective shape and cross-sectional size optimization

*Original*

In silico biomechanical design of the metal frame of transcatheter aortic valves: multi-objective shape and cross-sectional size optimization / Carbonaro, Dario; Gallo, Diego; Morbiducci, Umberto; Audenino, Alberto; Chiastra, Claudio. - In: STRUCTURAL AND MULTIDISCIPLINARY OPTIMIZATION. - ISSN 1615-147X. - ELETTRONICO. - (2021). [10.1007/s00158-021-02944-w]

*Availability:*

This version is available at: 11583/2904516 since: 2021-06-06T15:24:36Z

*Publisher:*

Springer

*Published*

DOI:10.1007/s00158-021-02944-w

*Terms of use:*

This article is made available under terms and conditions as specified in the corresponding bibliographic description in the repository

*Publisher copyright*

Springer postprint/Author's Accepted Manuscript

This version of the article has been accepted for publication, after peer review (when applicable) and is subject to Springer Nature's AM terms of use, but is not the Version of Record and does not reflect post-acceptance improvements, or any corrections. The Version of Record is available online at: <http://dx.doi.org/10.1007/s00158-021-02944-w>

(Article begins on next page)



# *In silico* biomechanical design of the metal frame of transcatheter aortic valves: multi-objective shape and cross-sectional size optimization

Dario Carbonaro<sup>1</sup> · Diego Gallo<sup>1</sup> · Umberto Morbiducci<sup>1</sup> · Alberto Audenino<sup>1</sup> · Claudio Chiastra<sup>1</sup>

Received: 25 November 2020 / Revised: 12 April 2021 / Accepted: 4 May 2021  
© The Author(s) 2021

## Abstract

Transcatheter aortic valve (TAV) implantation has become an established alternative to open-heart surgical valve replacement. Current research aims to improve the treatment safety and extend the range of eligible patients. In this regard, computational modeling is a valuable tool to address these challenges, supporting the design phase by evaluating and optimizing the mechanical performance of the implanted device. In this study, a computational framework is presented for the shape and cross-sectional size optimization of TAV frames. Finite element analyses of TAV implantation were performed in idealized aortic root models with and without calcifications, implementing a mesh-morphing procedure to parametrize the TAV frame. The pullout force magnitude, peak maximum principal stress within the aortic wall, and contact pressure in the left ventricular outflow tract were defined as objectives of the optimization problem to evaluate the device mechanical performance. Design of experiment coupled with surrogate modeling was used to define an approximate relationship between the objectives and the TAV frame parameters. Surrogate models were interrogated within a fixed design space and multi-objective design optimization was conducted. The investigation of the parameter combinations within the design space allowed the successful identification of optimized TAV frame geometries, suited to either a single or groups of aortic root anatomies. The optimization framework was efficient, resulting in TAV frame designs with improved mechanical performance, ultimately leading to enhanced procedural outcomes and reduced costs associated with the device iterative development cycle.

**Keywords** Transcatheter aortic valve implantation · Self-expandable devices · Finite element analysis · Cardiovascular device design · Shape and size optimization · Computational structural mechanics

## 1 Introduction

Transcatheter aortic valve (TAV) implantation has become an established clinical procedure that provides a minimally invasive alternative to open heart surgical valve replacement in medium- to high-risk elderly patients with calcific aortic valve disease and severe aortic stenosis (Tabata et al. 2019). Currently, there are approximately 180,000 potential candidates for TAV replacement in the European Union and in

Northern America annually, expecting an increase in number in the next years (Durko et al. 2018). Due to its minimally invasive approach and ongoing success, TAV replacement could become the standard treatment also for low-risk patients (Howard et al. 2019), leading to a fast expansion of new TAV designs (Fanning et al. 2013).

TAVs are generally composed by a bioprosthetic valve sutured on a metal frame (or stent) and can be grouped into balloon-expandable and self-expandable valves, featured by a stainless-steel and Nitinol frame, respectively (Dasi et al. 2017). TAVs are designed to be crimped into a catheter, delivered during the implantation procedure through the aorta and placed on the patient's diseased aortic valve to restore its native functionality (Jones et al. 2017). Considerable technological advances were conducted to improve the performance and safety of TAVs, although several complications still affect the potential of the treatment and are becoming of

---

Responsible Editor: Yoojeong Noh

✉ Claudio Chiastra  
claudio.chiastra@polito.it

<sup>1</sup> PoliTo<sup>BIO</sup>Med Lab, Department of Mechanical and Aerospace Engineering, Politecnico di Torino, Corso Duca degli Abruzzi, 24, 10129 Turin, Italy

more concern with the expansion to younger and lower-risk patients (De Biase et al. 2018). The most common complications affecting the current generation of TAV devices include postoperative paravalvular leak (PVL), conduction abnormalities, and valve thrombosis (Rotman et al. 2018). Additionally, aortic root damage and prosthesis migration, which are typically associated with the mutual interaction between the TAV and the aortic root, may occur (Neragi-Miandoab and Michler 2013).

The design of a TAV frame is a challenging task as it involves the fulfillment of multiple requirements. From a biomechanical viewpoint, TAVs should: (1) assure proper apposition to avoid PVL (Wang et al. 2012; Morganti et al. 2014; Tanaka et al. 2018), (2) generate low contact pressures to exclude conduction abnormalities (Rocatello et al. 2019), (3) produce low stress within the aortic root to limit the tissue damage (Auricchio et al. 2014; Morganti et al. 2014; Wang et al. 2015; Finotello et al. 2017; McGee et al. 2019a), and (4) exert an adequate pullout force to prevent valve migration (Mummert et al. 2013; Tzamtzis et al. 2013; McGee et al. 2019b). Among the arsenal of available tools supporting not only the design phase of TAVs, with the evaluation and optimization of their mechanical performance (Dasi et al. 2017), but also the definition of the optimal TAV implantation procedure (Schultz et al. 2016), *in silico* modeling (Luraghi et al. 2021), mainly based on the finite element (FE) method, assures the achievement of effective results with reduced time and costs as compared to a pure experimental approach. In particular, FE modeling represents the elective tool for achieving the optimization of the TAV frame geometry. Recently, a computational framework based on patient-specific aortic root models was proposed to successfully optimize the geometry of a commercial self-expandable TAV frame (Rocatello et al. 2019). However, the study was limited to the optimization of the TAV inflow portion. In order to improve the effectiveness of the optimization procedure, all the parameters associated with the overall TAV frame geometry should be considered, aiming to provide a comprehensive understanding of the relation between the TAV design and the post-procedural outcomes.

In the present study, a multi-objective shape optimization framework is presented, based on FE modeling of TAV frame implantation in an idealized aortic root anatomical model. The final goal is to contribute to improve the mechanical behavior of a TAV frame by using an approach that concurrently assures (1) reduced costs associated with the device iterative development cycle and (2) improved post-procedural outcomes. Technically, the design of the experiment method coupled with surrogate modeling was adopted here to explore the biomechanical interactions between different TAV designs and the aortic root. This allowed to define approximate relationships between optimization objectives, associated to postoperative complications, and design parameters of the

entire TAV frame geometry, ultimately leading to the identification of optimal TAV frame designs from the biomechanical viewpoint.

## 2 Methods

The procedure applied for shape and cross-sectional size optimization of a TAV frame consisted of the following main steps (Fig. 1): (1) FE modeling of TAV implantation procedure including an idealized aortic root model and a conventional Nitinol TAV frame model parametrized through a mesh-morphing procedure, (2) formulation of the optimization problem through the definition of the optimization objectives and feasible solution space, (3) coupling the design of the experiment method with the surrogate modeling approach to define an approximate relationship between optimization objectives and design parameters, and (4) identification of the optimal geometric attributes of the TAV frame. Each step of the present workflow is detailed in the following subsections.

### 2.1 Aortic root model

An idealized FE model of the human aortic root including a portion of the ascending aorta, the left ventricular outflow tract (LVOT), and the native aortic valve leaflets was created using Hypermesh (Altair Engineering, Troy, MI, USA) in conjunction with Abaqus/Standard (Dassault Systèmes Simulia Corp., Johnston, RI, USA) (Fig. 2a). The anatomical features of the model were based on previous studies (Labrosse et al. 2006; Auricchio et al. 2011; Formato et al. 2018). Specifically, the aortic anulus and LVOT diameters were set to 25 mm and the ascending aorta diameter to 30 mm. Additional dimensions are reported in Fig. 1-Suppl. A homogeneous thickness of 1.5 and 0.5 mm was assigned to the aortic root and the leaflets, respectively. Calcific and non-calcific aortic root models were generated. Calcifications were modeled as idealized structures. Based on previous experimental findings (Thubriker et al. 1986), the geometrical pattern of human calcific deposits was classified into two main categories here referred as pattern I, characterized by an arc shape located along the leaflet coaptation line (Fig. 2b), and pattern II, arc shaped and located along the leaflet attachment line (Fig. 2c) (Thubriker et al. 1986; Luraghi et al. 2020). Maximum thickness value (5 mm) and volume (1100 mm<sup>3</sup>) of the idealized calcifications were set based on data from patients suffering from aortic stenosis (Sturla et al. 2016; Pawade et al. 2018). An isotropic, incompressible hyperelastic Mooney-Rivlin material model (Table 1) was adopted to describe the mechanical behavior of the aortic root (Auricchio et al. 2011; Gunning et al. 2014). An elasto-plastic material model with perfect plasticity (Table 1) was employed to model the mechanical behavior of the calcific deposits (Bosi et al. 2018). The aortic root and the

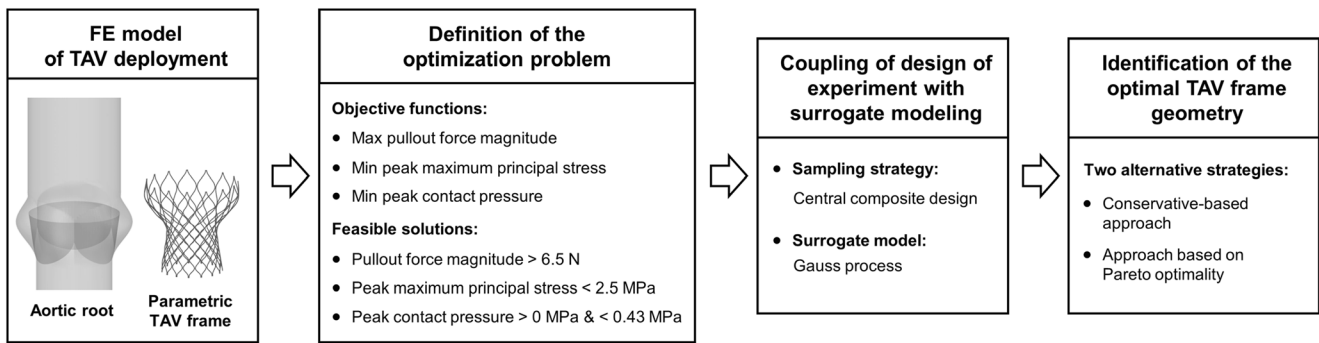


**Fig. 1** Main steps of the optimization framework: (1) FE modeling of TAV implantation procedure; (2) formulation of the optimization problem, defining optimization objectives, and feasible solutions; (3)

design parameters sampling and implementation of surrogate models of the optimization objective; and (4) identification of optimal TAV frame candidates

leaflets were discretized using four-node shell elements with reduced integration S4R, as justified by their thin geometry with constant thickness (Bosi et al. 2018) and calcifications were meshed using four-node tetrahedral elements C3D4 (Morganti et al. 2016; Bosi et al. 2018; McGee et al. 2019a). Tied contact was modeled between leaflets and the aortic root, as well as between leaflets and calcium deposits (Ovcharenko et al. 2016; Bosi et al. 2018).

The following three different scenarios were investigated: (1) aortic root without calcifications (in the following referred to as healthy configuration) (Fig. 2a), (2) diseased aortic root presenting pattern I calcifications (in the following referred to as diseased I configuration) (Fig. 2b), and (3) diseased aortic root presenting pattern II calcifications (in the following referred to as diseased II configuration) (Fig. 2c).

## 2.2 TAV frame model

A FE element model resembling the 29-mm CoreValve TAV (Medtronic, Dublin, Ireland) was created (Fig. 2d) using Hypermesh and Abaqus/Standard. The model was simplified by considering only a Nitinol frame composed by 30 strings and neglecting the porcine pericardial tissue valve, which has a marginal structural role (Bailey et al. 2016). Shape and dimensions of the TAV frame were retrieved from the

manufacturer data-sheet and from literature (Rocatello et al. 2019). The mechanical behavior of the Nitinol alloy was described implementing in Abaqus a super-elastic constitutive model (Auricchio and Taylor 1997) through a user-defined subroutine. The material parameters, retrieved from a previous study (Morganti et al. 2016), are summarized in Table 2. In accordance with previous computational studies (Gessat et al. 2014; Hopf et al. 2017; Rocatello et al. 2018, 2019), the TAV frame geometry was meshed using B31 Timoshenko beam elements, defining a local coordinate system for each element to properly orient the beam cross-section. This modeling choice was motivated not only by the device geometry, composed of slender strings, but also by the necessary compromise between computational efficiency and adequate accuracy of the results, as well as by the suitability of these elements to parametrized stent models generation (Hall and Kasper 2006).

## 2.3 Parametrization of the TAV frame model

The nominal geometry of the TAV frame was parametrized as a combination of four different morphing shapes (i.e., *shapes 1–4*, Fig. 3) by using a mesh-morphing approach in Hypermesh. Moreover, thickness and width of the beam cross-section were accounted as two additional size parameters. The design space of the six parameters was defined by properly setting a search space for each morphing shape (according to a normalized shape factor  $sf$ ) and size parameter. To do that, preliminary studies were conducted to identify degenerate geometries and convergence issues in the FE analyses of TAV deployment for the implemented shape combinations (Li et al. 2009; Wu et al. 2010).

The four mesh-morphing shapes were introduced to parametrize the whole TAV frame geometry in terms of radial and axial dimensions and, at the same time, to consider separately the morphing of the upper and lower parts of the TAV frame with two independent parameters. More in detail, *shapes 1* and *3* varied the total height of the frame and the radial position of all the nodes, according to a shape factor  $sf_1$  and  $sf_3$  within the ranges  $[0, 1]$  and  $[-1, 1]$ , respectively (Fig. 3).

**Table 1** Aortic root and calcium deposits material parameters (Auricchio et al. 2011; Gunning et al. 2014; Bosi et al. 2018)

Aortic root material parameter	Value
Mooney-Rivlin constant $C_{10}$	0.55 MPa
Mooney-Rivlin constant $C_{01}$	0.14 MPa
Incompressibility parameter	$10^{-6}$
Calcium deposits material parameter	Value
Young's modulus	400 MPa
Poisson's ratio	0.3
Yielding stress	0.4 MPa

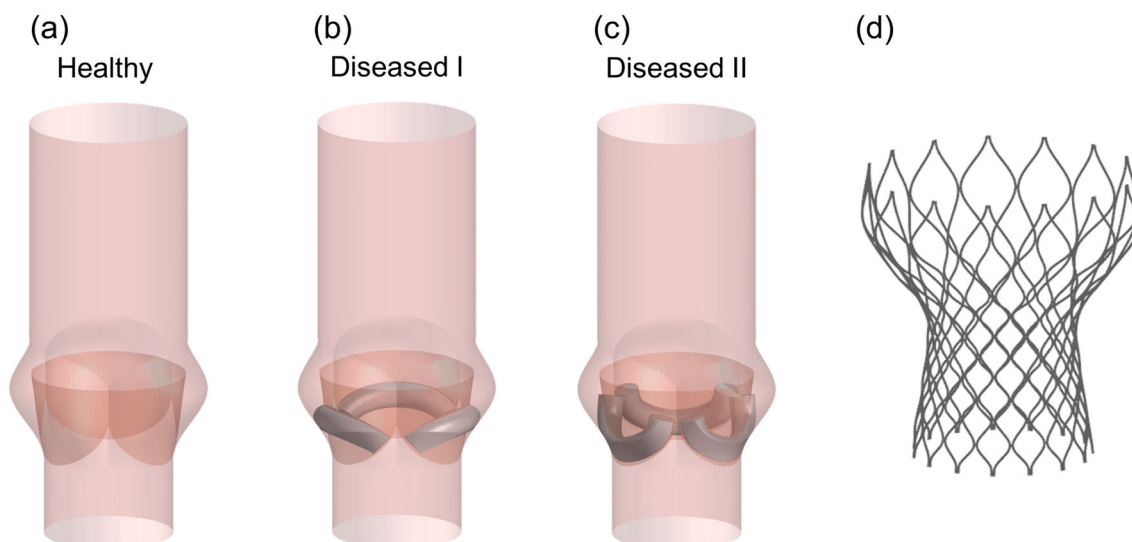


**Fig. 2** Idealized FE models of the human aortic root and of the TAV frame. **a** “Healthy” aortic root model without calcific deposits, **b** and **c** “Diseased I” and “diseased II” aortic root models, respectively, according to the idealized calcium patterns I and II (Thubrikar et al. 1986). **d** TAV frame

Shapes 2 e 4 were defined by folding the TAV frame geometry to a cylinder with a diameter equal to the minimum TAV frame diameter, varying the top and bottom of the TAV frame diameter, respectively, according to a shape factor  $sf_2$  and  $sf_4$  with range  $[-1, 1]$  (Fig. 3).

In addition to the four shapes, the thickness and width of the TAV frame string cross-section (nominal values of 0.25 and 0.45 mm) were varied within ranges  $[0.15 \text{ mm}, 0.35 \text{ mm}]$  and  $[0.35 \text{ mm}, 0.55 \text{ mm}]$ , respectively. The links between the strings were assumed to have the same string thickness and a width equal to 1.5-fold the string width.

## 2.4 Finite element analyses of TAV implantation

FE analyses of the TAV implantation procedure were performed using the implicit code Abaqus/Standard to solve the non-linear equations of static equilibrium on 6 computing cores of a workstation equipped with Intel® Core™ i7-8700

and 32 GB RAM. Two procedural steps were simulated (Table 3). In the first step, the TAV frame insertion into the catheter capsule, modeled as two concentric rigid cylindrical surfaces (Cabrera et al. 2017), was carried out (Fig. 4a, b, Video 1-Suppl). In the second step, the device was released and placed in contact with the aortic root (Fig. 4c, d, Video 1-Suppl). Due to the angular symmetry of the model (see Fig. 2), only one third of the aortic root, frame, and catheter were modeled and symmetry boundary condition were applied accordingly. Interactions between the parts were implemented with the contact-pair algorithm, based on a master-slave approach, considering the default “hard” normal contact behavior with a friction coefficient of 0.09 for the TAV frame/aortic root and TAV frame/catheter capsule interaction, and a friction coefficient of 0.36 for the frame/calcium and aortic root/calcium (McGee et al. 2019b). Artificial damping was added to stabilize the non-linear simulations, controlling that the ratio between the related dissipation energy and total internal energy was less than 5% (Abaqus 2016). Nodes at the lower extremity of the TAV frame were positioned 4 mm under the aortic anulus plane (Fig. 4c), in accordance with the procedural guidelines defined by the device manufacturer (Medtronic 2014) and were constrained in the vessel axis direction, as well as nodes on the upper and lower edges of the aortic root (Fig. 4c). In the crimping simulation step, the external rigid cylinder was radially crimped from a diameter of 100 to 6 mm, while the internal cylinder remained fixed to a diameter of 5 mm, in accordance with the catheter capsule dimensions provided by the device manufacturer (Medtronic 2014). In the release simulation step, the external cylinder was released to its initial diameter (i.e., 100 mm) to allow for the contact between the TAV frame and the aortic root model.

A mesh independence analysis was carried out before the execution of the optimization study by progressively doubling

**Table 2** TAV frame Nitinol material parameters (Morganti et al. 2016)

Material parameter	Value
Austenite elastic modulus	51,700 MPa
Martensite elastic modulus	47,800 MPa
Poisson’s ratio	0.3
Start of transformation loading	600 MPa
End of transformation loading	670 MPa
Start of transformation unloading	288 MPa
End of transformation unloading	254 MPa
Maximum transformation strain	6.3%
Maximum volumetric transformation strain	6.3%
Reference temperature	37°

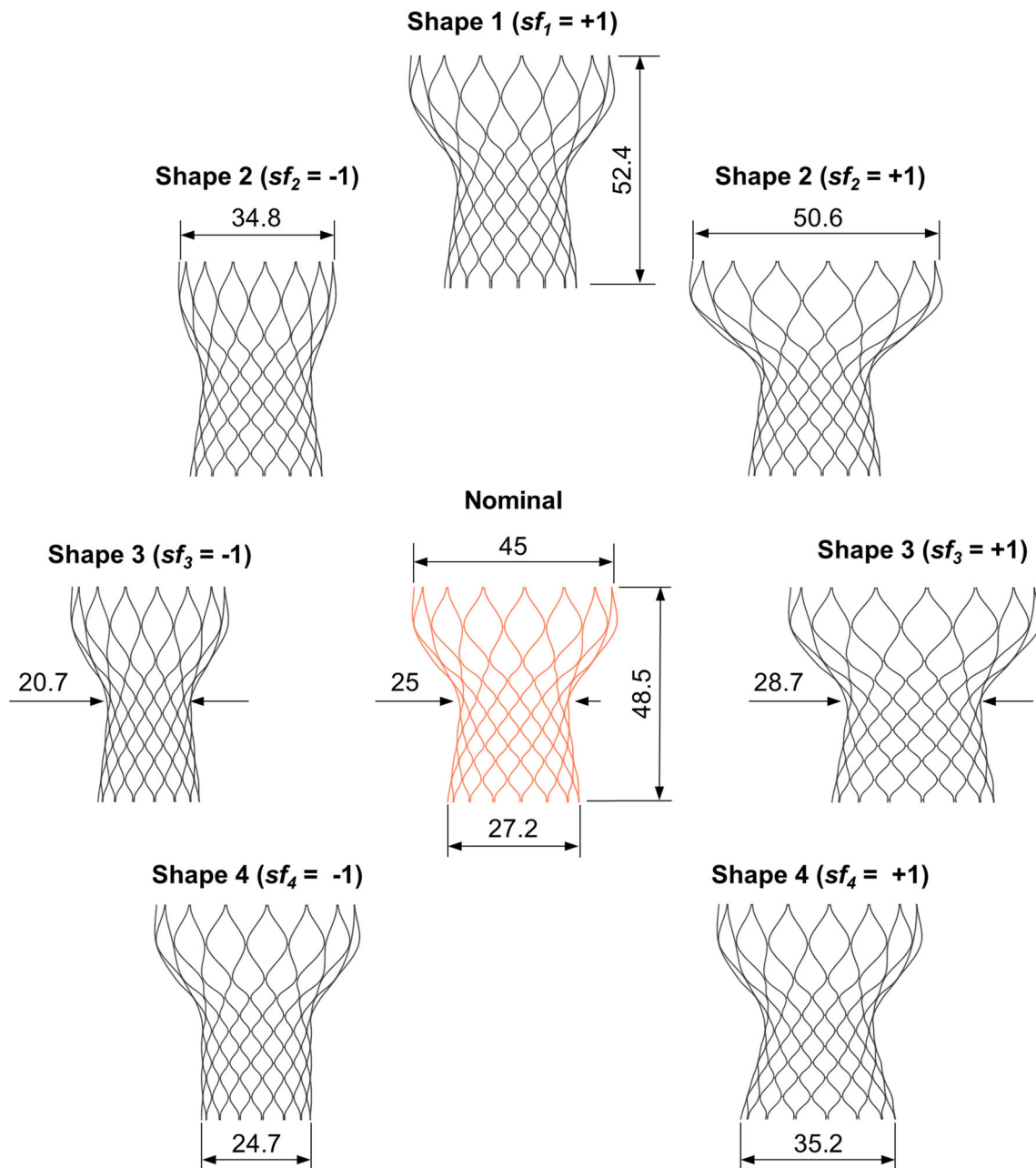


**Fig. 3** Parametrization of the nominal geometry of the TAV frame (in orange) as a combination of four mesh-morphing shapes (i.e., shapes 1–4). For each morphing shape, both normalized shape factors ( $sf_i$  with  $i = 1,$

2, 3, 4) and the corresponding dimensions, identifying the range of each design parameter, are reported. Dimensions are indicated in millimeters

the mesh element size. The results were assumed mesh independent when the difference between the solution of two consecutive mesh refinements was less than 3% in terms of pull-out force magnitude exerted by the device and peak maximum principal stress within the aortic wall, and less than 10% in terms of peak contact pressure. As a result, a mesh cardinality of 23,408 S4R shell elements for the aortic root, 2110 B31 beam elements for the TAV frame, 20,764 SFM3D4R surface elements for the catheter, 23,266 and 35,967 C3D4 tetrahedral elements for the calcification patterns I and II, respectively, were adopted.

## 2.5 Optimization procedure

### 2.5.1 Optimization objectives and constraints

The optimization of the biomechanical performance of the device and the related effectiveness of the TAV implantation procedure consisted in minimizing the risk of migration, tissue damage, and conduction abnormalities associated with TAV replacement and, hence, involved the maximization of the pullout force magnitude (defined as the resultant of the normal contact forces acting on all nodes of the TAV frame multiplied

**Table 3** Summary and description of the steps of FE analysis of the TAV implantation

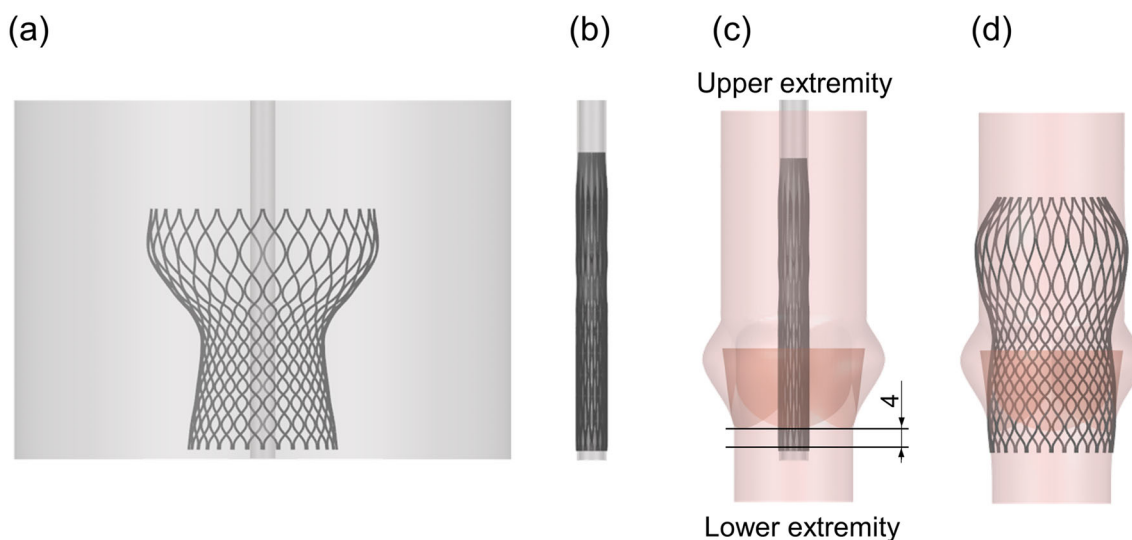
Step	Description	Contacts	Boundary conditions
1	TAV frame crimping into the catheter	TAV frame/catheter Aortic root/calcium deposits	External rigid cylinder diameter: from 100 to 6 mm Internal rigid cylinder fixed in all directions Lower extremity of the TAV, upper and lower edges of the aortic root fixed in the vessel axis direction Angular symmetry of the FE model
2	TAV frame release into the aortic root	TAV frame/catheter TAV frame/aortic root TAV frame/calcium deposits Aortic root/calcium deposits	External rigid cylinder diameter: from 6 to 100 mm Internal rigid cylinder fixed in all directions Lower extremity of the TAV, upper and lower edges of the aortic root fixed in the vessel axis direction Angular symmetry of the FE model

by their corresponding friction coefficient), the minimization of the peak maximum principal stress and peak contact pressure, respectively. In detail, the optimization problem was performed according to the following constraints, which defined the feasible solution space:

- (1) The pullout force magnitude exerted by the device should be greater than 6.5 N, a value proposed as the lower limit for avoiding the migration of the device (Mummert et al. 2013; Tzamtzis et al. 2013; McGee et al. 2019b).
- (2) The peak value of the maximum principal stress within the tissue, considered as a measure of the risk of damage of the aortic root tissue (Auricchio et al. 2014; Morganti et al. 2014; Wang et al. 2015; Finotello et al. 2017; McGee et al. 2019a), should be lower than 2.5 MPa, which has been proposed as the material limit for the occurrence of tissue tearing (Wang et al. 2015).
- (3) The peak value of the contact pressure in the atrioventricular conduction system, considered as a measure of the risk for rhythm disturbances (Rocatello et al. 2018), should be lower than 0.43 MPa, which has been

proposed as the upper limit value for the occurrence of conduction abnormalities (Rocatello et al. 2018). It must be noted that, differently from previous studies (Rocatello et al. 2018) where the atrioventricular conduction system was located in the LVOT of patient-specific models using computed tomography data, in the present study, the atrioventricular conduction system location could not be precisely defined as an idealized aortic root model was investigated. For this reason, the contact pressure was conservatively computed in the entire LVOT. Additionally, the risk of PVL, which occurs when the device is not completely in contact with the aortic root at the level of the LVOT, was accounted for by applying a further constraint to the peak contact pressure objective: peak contact pressure values under the anulus plane should be greater than zero, to guarantee the contact between the TAV frame and the aortic root wall. Therefore, solutions with non-null contact pressure in the LVOT are desirable to avoid PVL.

Summarizing, the present optimization problem can be mathematically formulated as:

**Fig. 4** FE analysis of the TAV implantation procedure. **a–b** Insertion of the TAV into the catheter capsule. **c–d** TAV release into the aortic root

$$\begin{cases} \max_{\mathbf{x} \in D} f_{PF}(\mathbf{x}) \\ \min_{\mathbf{x} \in D} f_{MPS}(\mathbf{x}) \\ \min_{\mathbf{x} \in D} f_{CP}(\mathbf{x}) \\ \text{s.t. : } \begin{cases} f_{PF}(\mathbf{x}) > 6.5 \text{ N} \\ f_{MPS}(\mathbf{x}) < 2.5 \text{ MPa} \\ 0 \text{ MPa} < f_{CP}(\mathbf{x}) < 0.43 \text{ MPa} \\ D = \left\{ \begin{array}{l} \mathbf{x} = [sf_1, sf_2, sf_3, sf_4, t, w] : sf_i \in [0, 1], \\ sf_i \in [-1, 1] \text{ with } i = 2, 3, 4, \\ t \in [0.15 \text{ mm}, 0.35 \text{ mm}], w \in [0.35 \text{ mm}, 0.55 \text{ mm}] \end{array} \right\} \end{cases} \end{cases} \quad (1)$$

where pullout force  $f_{PF}$ , peak maximum principal stress  $f_{MPS}$ , and peak contact pressure  $f_{CP}$  are the optimization objectives;  $\mathbf{x}$  is the vector of the design parameters;  $D$  is the design space;  $sf_1, sf_2, sf_3, sf_4$  are the shape factors associated to the mesh-morphing shapes of the TAV frame model, and the thickness  $t$  and width  $w$  are the cross-sectional size parameters.

### 2.5.2 Surrogate modeling

Separate surrogate models were constructed for each objective within the multi-objective optimization framework. The central composite design (*circumscribed*) sampling strategy (Draper and Lin 1996) was implemented in Hyperstudy (Altair Engineering, Troy, MI, USA), running 77 sampling FE simulations of TAV implantation for each aortic root configuration. The number of samples was defined by the following formula (Draper and Lin 1996):

$$2^k + 2k + n_0 \quad (2)$$

where  $k$  is the number of design parameters ( $k = 6$ ) and  $n_0$  is the number of center points ( $n_0 = 1$ ).

On the conducted simulations, optimization objectives were computed and the output data were exported in Matlab (Mathworks, Natick, MA, USA). Gauss process surrogate models (Rasmussen and Williams 2018) were adopted in Matlab to define an approximate relationship between the six design parameters and the optimization objectives. This combination of sampling strategy and surrogate model was selected after a preliminary analysis that compared the central composite design and Gauss process surrogate model against other combinations involving the Latin hypercube sampling strategy (McKay et al. 1979) and the polynomial surrogate model (Draper and Lin 1996), which were previously used for the design optimization of endovascular devices (Li and Wang 2013; Clune et al. 2014; Bressloff et al. 2016; Alaimo et al. 2017; Rocatello et al. 2019). Details about this preliminary study are reported in the [Supplementary materials](#). The validity of the models was assessed with the leave-one-out principle, plotting each predicted value in function of the simulated value and evaluating the overall validation error in

terms of predicted coefficient of determination  $R_{pred}^2$ . Furthermore, a consistency check was performed by verifying that computed standardized cross validated residual (SCVR) values lied within the  $[-3, 3]$  range (Jones et al. 1998; Pant et al. 2012).

### 2.5.3 Multi-objective optimization

The selection of the optimal TAV frame geometry, even after obtaining the surrogate models and defining the feasible solution space, is not straightforward and several approaches can be applied to finalize the optimization process (Pant et al. 2011). In this study, the multi-objective optimization problem was initially considered as unconstrained. The constraints were applied in a second stage to identify optimal candidate geometries within the feasible solution space. In detail, two alternative approaches were adopted.

First, a conservative-based approach was applied, in which optimal candidates were considered to remain in the middle region of the feasible solution space defined by the objective constraints, thereby avoiding poor performance of the device in any of the objectives. Specifically, the surrogate models were used to predict the objectives for each possible combination of design parameters  $\mathbf{x}$  within a discretized design space (six parameters, eight samples within each parameter range). Three margins of safety, each related to one objective and based on its constraint values, were defined as:

$$MS_{PF}(\mathbf{x}) = \frac{f_{PF}(\mathbf{x})}{6.5 \text{ N}} - 1 \quad (3)$$

$$MS_{MPS}(\mathbf{x}) = 1 - \frac{f_{MPS}(\mathbf{x})}{2.5 \text{ MPa}} \quad (4)$$

$$MS_{CP}(\mathbf{x}) = \min \left( 1 - \frac{f_{CP}(\mathbf{x})}{0.43 \text{ MPa}}, \frac{f_{CP}(\mathbf{x})}{0.43 \text{ MPa}} \right) \quad (5)$$

where  $MS_{PF}(\mathbf{x})$ ,  $MS_{MPS}(\mathbf{x})$ , and  $MS_{CP}(\mathbf{x})$  are the margins of safety related to pullout force, peak maximum principal stress, and peak contact pressure, respectively. Then, an overall margin of safety  $MS(\mathbf{x})$  was computed as:

$$MS(\mathbf{x}) = \min(MS_{PF}(\mathbf{x}), MS_{MPS}(\mathbf{x}), MS_{CP}(\mathbf{x})). \quad (6)$$

Among all the combinations of design parameters, the one that guaranteed the largest overall margin of safety  $MS(\mathbf{x})$  was conservatively identified as optimal TAV frame candidate. This approach was applied twice (1) considering separately the healthy, diseased I, and diseased II configurations, to identify the optimal TAV frame geometry for the specific anatomy, and (2) considering simultaneously the two “diseased” configurations, to identify an optimal TAV frame geometry implantable in a wider range of diseased anatomies. Hence, four optimal TAV frame geometry candidates were searched.

Secondly, an approach based on Pareto optimality was applied to generate sets of optimal candidate geometries, ensuring high flexibility over the device design process, for which multiple desirable characteristics (e.g., hemodynamics features, manufacturing-related aspects, reduced costs) have to be considered in addition to the mechanical performance. Accordingly, the non-dominated sorting genetic algorithm (NSGA-II) (Deb et al. 2002), one of the most popular, reliable, fast sorting, and elite multi-objective genetic algorithm, suitable to identify Pareto-optimal solutions (Yusoff et al. 2011), was used in the Matlab environment. Technically, a population of 200 individuals, a binary tournament selection, a cross-over fraction of 0.8, and a Gaussian mutation were chosen for the multi-objective optimization problem, considering a maximum number of 600 generations. Sets of non-dominated-optimal solutions were identified for the three objectives, so that an improvement in one objective could only be the result of the worsening of at least one of the other objectives. Subsequently, feasible solutions were identified within the Pareto front by considering the objectives constraint, according to the approach already proposed in the past for stent design optimization (Pant et al. 2011). Due to the high computational costs required, consistency check of the Pareto front was conducted by performing the corresponding FE analyses for three Pareto-optimal solutions for each aortic root configuration, selected at the extremes and at the center of the Pareto front. Predicted objective values were plotted in function of the corresponding simulated values, checking the feasibility and optimality of the solutions.

### 3 Results

#### 3.1 Nominal TAV frame geometry

Figure 5 shows the simulation outputs related to the three optimization objectives of interest in the case of the nominal TAV frame geometry virtually implanted in the three different aortic root configurations. Considering the healthy configuration (Fig. 5a, left panel), normal contact forces were mostly exerted from the aortic root to the TAV frame in the LVOT, generating a total pullout force magnitude equal to 2.3 N. Differently, for both diseased I and diseased II configurations (Fig. 5a, central and right panels), normal contact forces were mainly exerted between the TAV frame and calcium deposits, resulting in a total pullout force magnitude equal to 16.9 and 19.5 N, respectively. The peak maximum principal stress within the aortic root was lower in absence of calcification (0.56 MPa vs. 1.91 MPa and 1.70 MPa for the healthy and diseased I and II configurations, respectively) (Fig. 5b). The peak contact pressure in the LVOT was higher in the healthy case than the diseased ones (0.66 MPa vs. 0.56 MPa and 0 MPa for the healthy and diseased I and II configurations,

respectively) (Fig. 5c). The null value of contact pressure occurring in the diseased II configuration indicated the absence of contact between the TAV frame and LVOT, revealing the presence of a minimum gap area of 7 mm<sup>2</sup>. According to a previous study reporting a correlation between the minimum cross-section gap area between the frame and the aortic anulus with the PVL volume (Tanaka et al. 2018), the computed minimum gap area of 7 mm<sup>2</sup> corresponded to a mild-to-moderate PVL.

#### 3.2 Objective functions trade-offs

Based on the 77 simulations samples and for each aortic root configuration, Fig. 6 summarizes the nature of the relationship between optimization objectives. According to the formulated optimization problem, the conflict between pullout force magnitude vs. peak maximum principal stress, and pullout force magnitude vs. peak contact pressure was observable for all the three configurations. This means that high pullout force magnitude values are effective in avoiding TAV migration, but they could lead to excessive peak maximum principal stress and peak contact pressure values, which are associated with an increased risk for tissue damage and conduction abnormalities, respectively (Wang et al. 2015; Dasi et al. 2017; Rocatello et al. 2019). The sample points related to the healthy configuration presented, on average, peak maximum principal stress and pullout force magnitude values lower than the “diseased” configurations (Fig. 6a, b). Furthermore, in the healthy configuration, the low generated pullout force magnitude and high peak contact pressures made sample points lied outside of the feasible solution space (Fig. 6b, transparent gray region), in contrast with the diseased configurations sample points. Thirty-two and 56 sample points related to the diseased I and II configurations, respectively, were characterized by null contact pressures (Fig. 6b, c), implying that the corresponding TAV frames were subjected to PVL when implanted in the calcified aortic root. In those cases, the associated minimum gap area was equal to 2.5 and 7.0 mm<sup>2</sup> for the diseased I and II configurations, respectively, highlighting the presence of a mild aortic regurgitation grade (Tanaka et al. 2018).

#### 3.3 Surrogate models

##### 3.3.1 Surrogate model validation

The results of the preliminary analysis conducted to select an adequate combination of sampling strategy and surrogate models are reported in the [Supplementary Materials](#). The combination of central composite design and Gauss process surrogate model emerged as the most effective to the aims of this study, and in the following all presented results are referred to this combination.

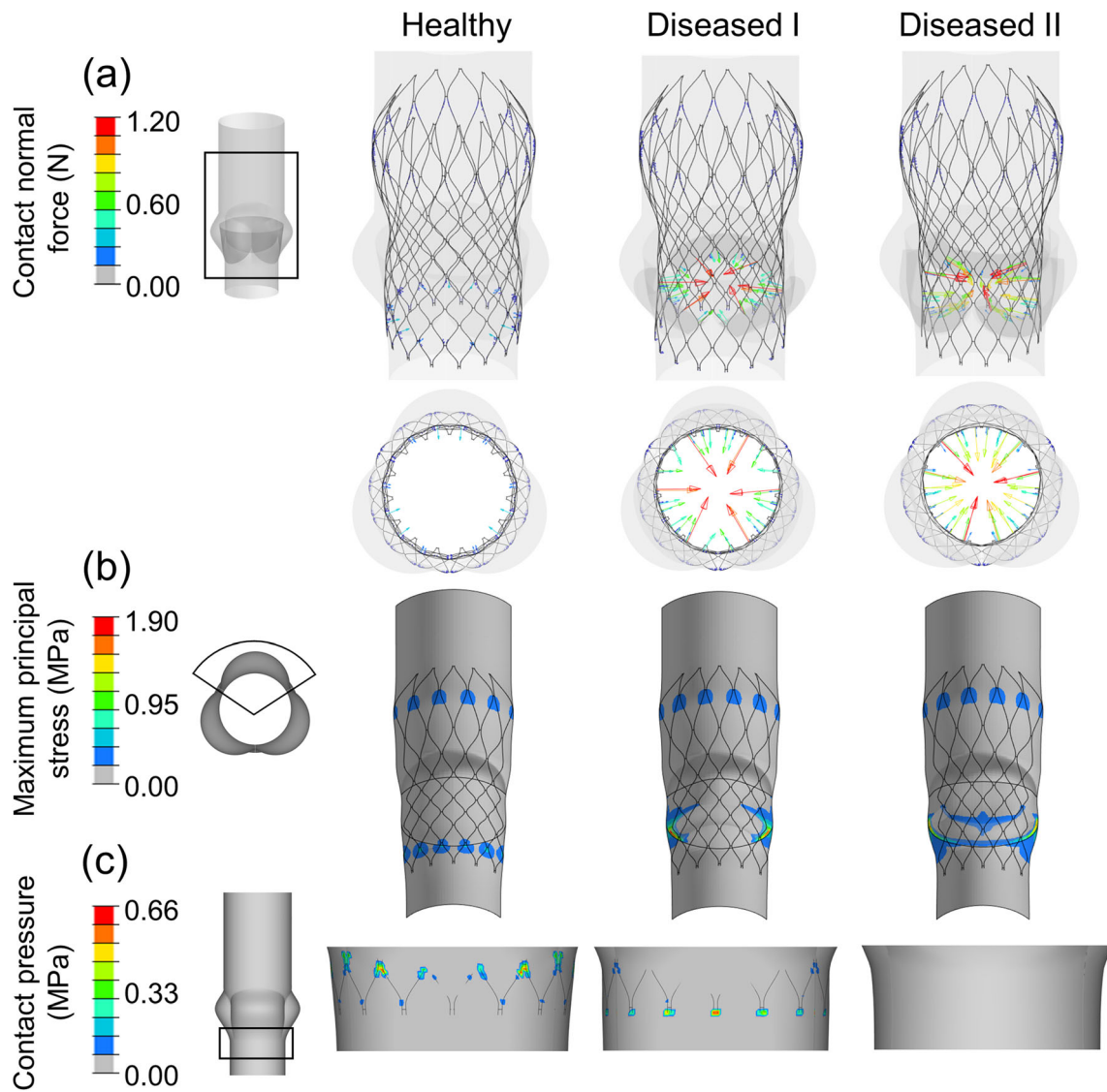


**Fig. 5** FE analysis outputs related to the three optimization objectives in the case of the nominal TAV frame geometry virtually implanted in the three aortic root configurations. **a** Contact normal forces computed on the

TAV frame. **b** Maximum principal stress computed within the aortic root wall. **c** Contact pressure computed in the LVOT

The output of the validation process of surrogate models, based on the leave-one-out principle, is summarized in Fig. 7, in which pullout force magnitude, peak maximum principal stresses, and peak contact pressures values predicted by the Gauss process vs. the corresponding simulated values are presented. The excellent agreement between predicted and simulated objective values (in the case of both healthy and diseased configurations) is confirmed by the strong direct proportionality of the data points, well aligned with the identity line, and by the very high values of the coefficient of determination ( $R^2_{pred} > 0.94$ ) (Table 4). Moreover, nearly all SCVR values of the predicted objectives lied within the required interval  $[-3, 3]$  (Pant et al. 2012) (Fig. 8), indicating the validity of the Gauss process surrogate models.

### 3.3.2 Geometry parameters exploration

The validated surrogate models were used to investigate the impact of each design parameter on the optimization objectives by varying two design parameters at time while maintaining the others fixed at the nominal value, as shown in Fig. 9.

The string cross-section parameters (i.e., thickness and width) and shape 3, which was related to the TAV frame overall radial dimension (Fig. 3), had major impact on pullout force magnitude, in particular in the case of the diseased configurations, where high values of those parameters were associated with high pullout force magnitude (Fig. 9a, upper and central panels). Differently, shape 1, which was related to the

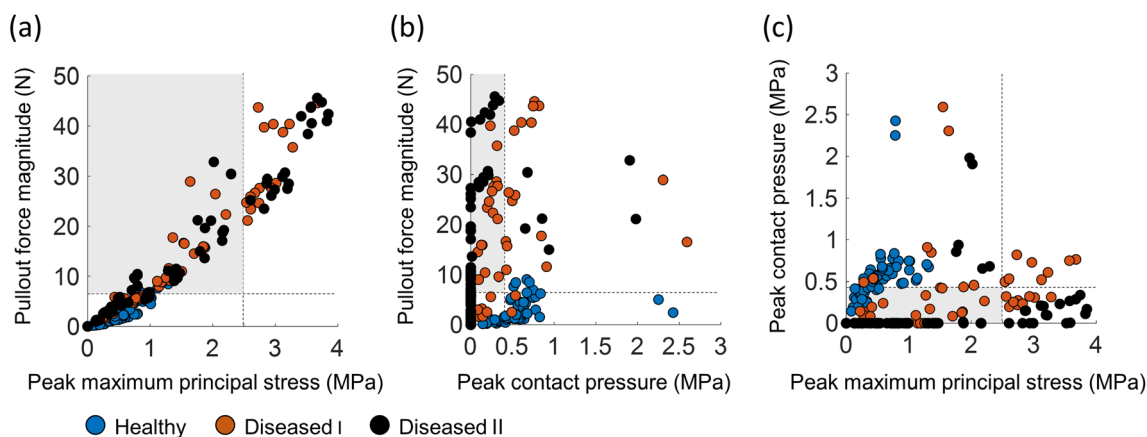


**Fig. 6** Simulated objectives trade-offs for the 77 simulation samples of the “healthy”, “diseased I”, and “diseased II” aortic root configurations. **a** Pullout force magnitude vs. peak maximum principal stress. **b** Pullout force magnitude vs. peak contact pressure. **c** Peak contact pressure vs.

peak maximum principal stress. Constraints of the objectives are indicated as dotted line, illustrating the feasible solution space as transparent gray region

TAV frame height (Fig. 3), had negligible impact on the pullout force magnitude (Fig. 9a, central panel). Shapes 2 and 4, which were related to the upper and lower parts of the TAV frame (Fig. 3), respectively, had an impact on the pullout force magnitude only for the diseased cases (Fig. 9a, bottom panel).

In all aortic root configurations, string width and shape 3 design parameters had major impact on the peak maximum principal stress (with the highest parameters value associated with the highest peak maximum principal stress values, Fig. 9b upper and central panel). Conversely, string thickness and shape 1 design parameters had a marginal impact on peak maximum principal stress values (Fig. 9b, upper and central panels). As for shape 2 and shape 4, those parameters had some impact on the peak maximum principal stress only in the case of healthy and diseased I configurations (Fig. 9b, bottom panel).

Thickness, width, shape 1, and shape 4 had a considerable impact on the peak contact pressure in the LVOT of both healthy and diseased I aortic root configurations (Fig. 9c). Shape 3 had some impact only on the healthy configuration (Fig. 9c, central panel), while shape 2 did not markedly influence the healthy and diseased I configurations (Fig. 9c, bottom panel). None of the design parameters influenced the peak contact pressure of the diseased II configuration, which was always equal to zero independent of the design parameter

combination (Fig. 9c), highlighting that in this case PVL could not be avoided by just combining two of the six design parameters of interest.

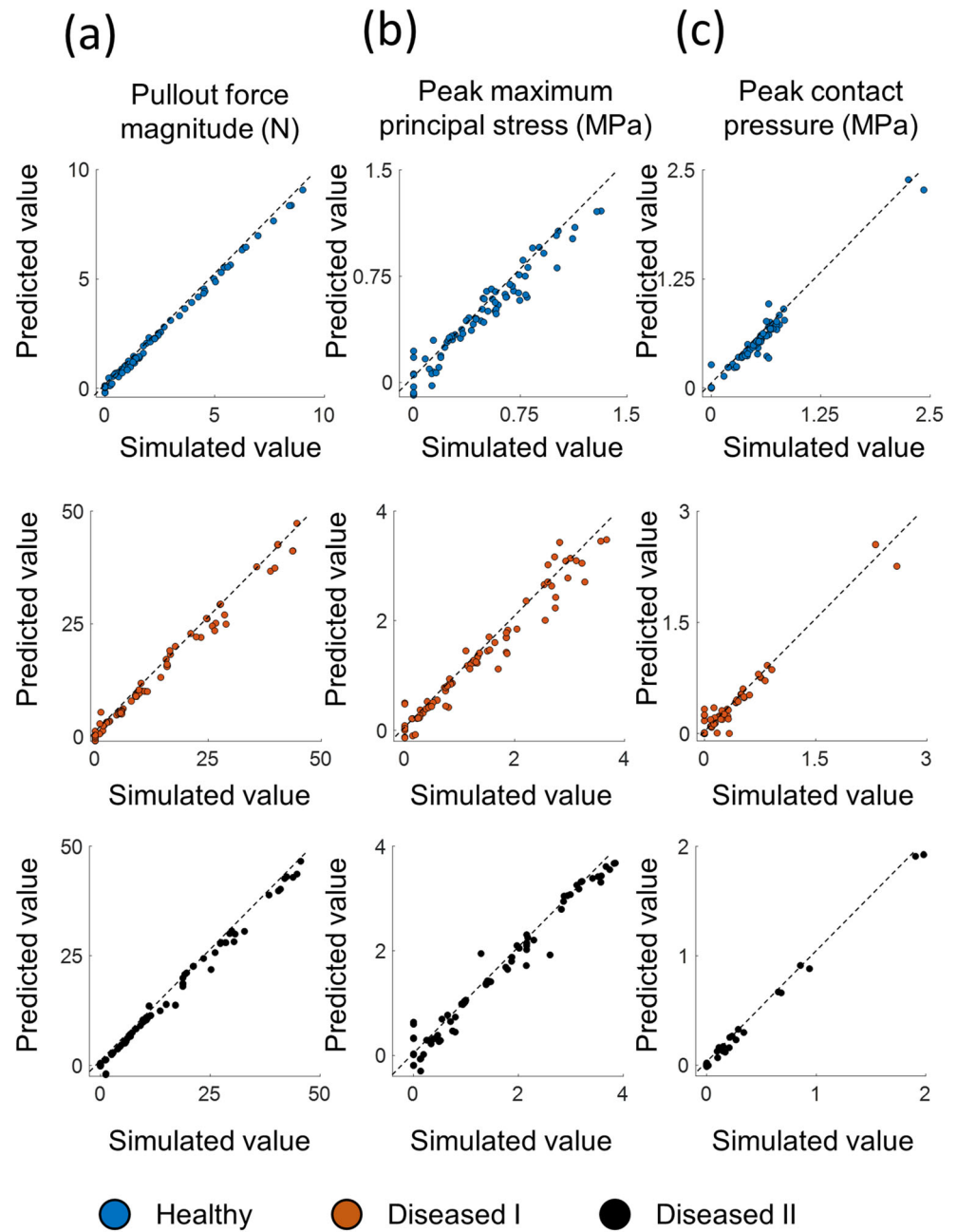
### 3.4 Choice of the optimal TAV frame geometry

The optimized TAV frame geometries and corresponding string cross-section values, obtained using the conservative constraint-based approach, are presented in Fig. 10 overlapped to the nominal geometry for the healthy (Fig. 10a, optimized 1), diseased I (Fig. 10b, optimized 2), and disease II (Fig. 10c, optimized 3) configurations, and considering the two diseased configurations simultaneously (Fig. 10d, optimized 4). The objective values of the optimized TAV frame geometries are summarized in Table 5 and compared to those related to the nominal geometry. In the case of the healthy configuration (i.e., optimized 1 TAV frame geometry), no feasible solution was generated, although a 137% beneficial increase of the pullout force magnitude and a 25% beneficial decrease of peak contact pressure was obtained with respect to the nominal geometry while maintaining the peak maximum principal stress still within the aortic root material limit (i.e., < 2.5 MPa (Wang et al. 2015)). Conversely, in the case of diseased configurations, optimized 2 and optimized 3 candidates identified objective values within the feasible solution space.

**Table 4** Coefficient of determination  $R^2_{pred}$  through cross-validation prediction of the objectives for the three aortic root configurations

	Aortic root		
	Healthy	Diseased I	Diseased II
$R^2_{pred}$ –Pullout force magnitude	0.99	0.94	0.96
$R^2_{pred}$ –Peak maximum principal stress	0.99	0.95	0.95
$R^2_{pred}$ –Peak contact pressure	0.99	0.97	0.99

**Fig. 7** Leave-one-out predicted values of the **a** pullout force magnitude, **b** peak maximum principal stress, **c** peak contact pressure in function of the corresponding simulated values, for the “healthy”, “diseased I”, and “diseased II” aortic root configurations

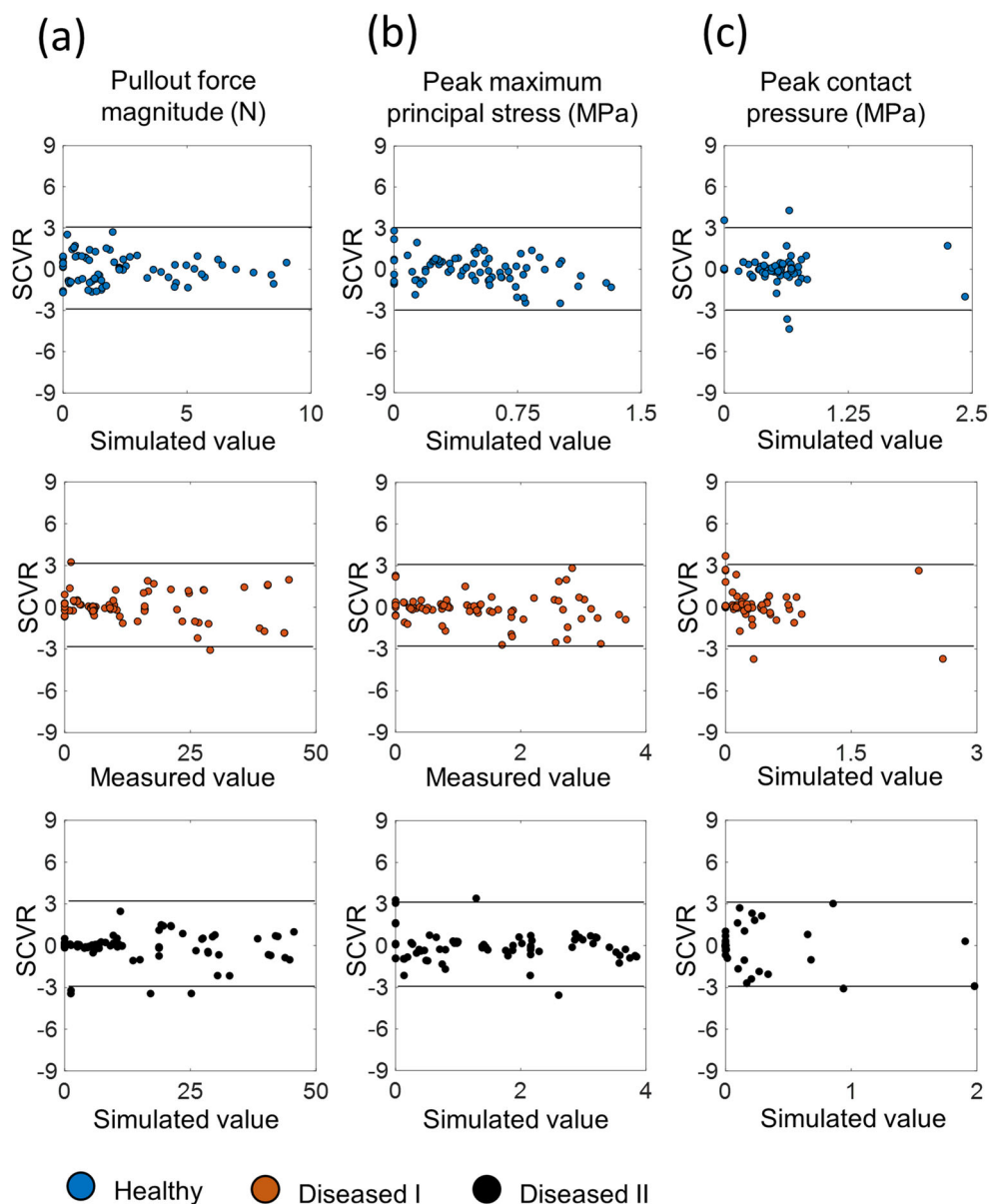


In detail, a beneficial outcome in terms of peak maximum principal stress and peak contact pressure was obtained, with pullout force magnitude lower than those of the nominal geometry but still conservatively higher than the minimum acceptable value of 6.5 N (Mummert et al. 2013; McGee et al. 2019b). Moreover, different from the corresponding values characterizing the nominal geometry, peak contact pressure values belonging to the feasible solution space (i.e., > 0 MPa and < 0.43 MPa (Rocatello et al. 2018)) were obtained. Considering the optimized 4 TAV frame geometry (i.e., the one associated with the two diseased aortic root configurations simultaneously), all quantities defined here as objective values

fell within the feasible space, although with a reduced margin of safety with respect to the geometries optimized 2 and optimized 3.

The sets of non-dominated optimal solutions lying on the Pareto front of the three objectives pullout force magnitude, peak contact pressure, and peak maximum principal stress are presented in the plane of pullout force magnitude vs. peak maximum principal stress in Fig. 11. All the Pareto-optimal solutions of the healthy aortic root configuration were found to be located outside of the feasible solution space (Fig. 11a). Conversely, acceptable Pareto-optimal solutions were present in the case of the diseased configurations (Fig. 11b, c).

**Fig. 8** SCRV values of the **a** pullout force magnitude, **b** peak maximum principal stress, and **c** peak contact pressure in function of the corresponding simulated values, for the “healthy”, “diseased I”, and “diseased II” aortic root configurations



However, differently from the diseased I configuration, a remarkable number of points of the diseased II configuration falling within the admissible region of peak maximum principal stress and pullout force magnitude exhibited unfeasible contact pressure values (Fig. 11).

The output of the consistency check of the Pareto front is presented in Fig. 12, which shows the predicted vs. simulated objective values for the selected Pareto-optimal solutions for each aortic root configuration. The three solutions were selected within the feasible space for the diseased configurations, whereas outside the feasible space for the healthy configuration. The consistency between simulated and predicted values was observable, with a direct proportionality of the data points, well aligned with the identity line, in particular in case of the healthy and diseased I aortic root configurations for all

the objectives and of the diseased II configuration for the pullout force magnitude and peak maximum principal stress.

## 4 Discussion

The application of computational modeling tools to the design process of endovascular devices, in particular in the initial proof-of-concept and prototyping phases, has been gaining a dramatically growing interest from the medical device industry (Morrison et al. 2017, 2018). Computational simulations can facilitate the design, optimization, and development phases of medical devices (Morrison et al. 2017), reducing the number of prototypes to be manufactured and the experimental tests, with positive impact on the product development

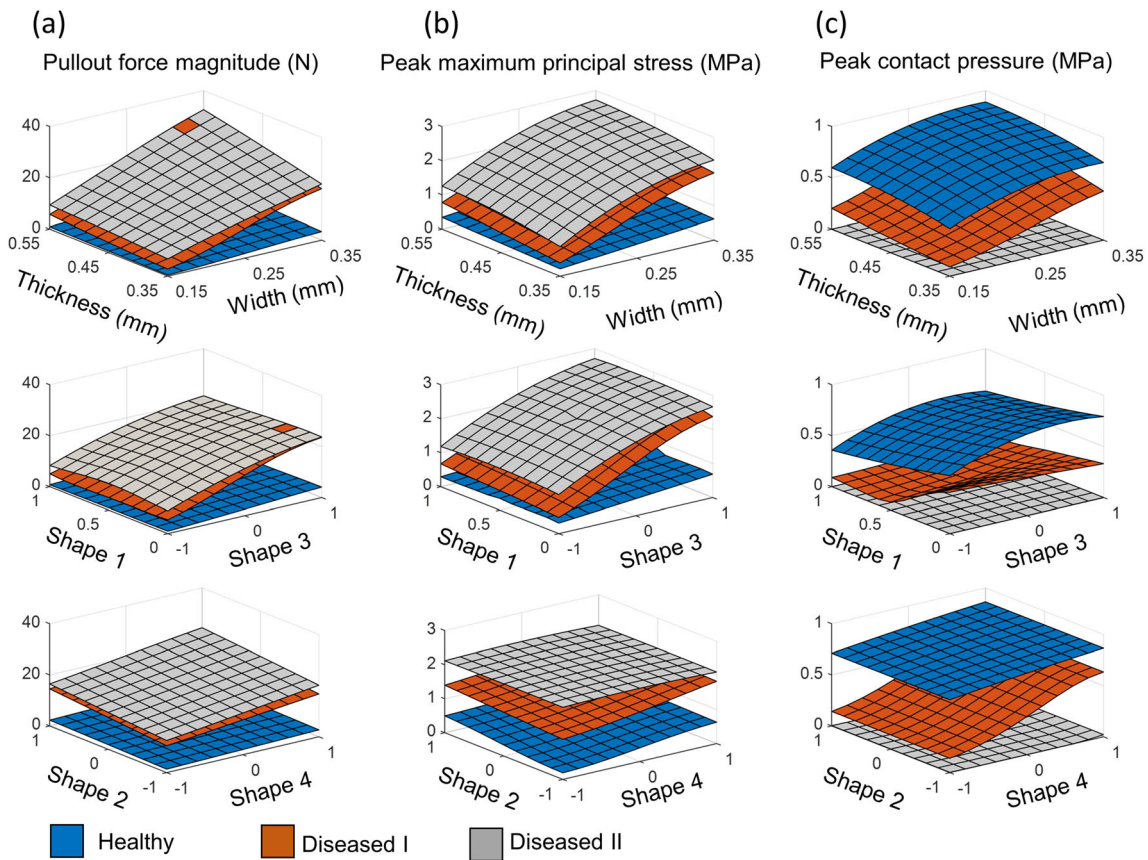


**Fig. 9** Predicted values of the **a** pullout force magnitude, **b** peak maximum principal stress, and **c** peak contact pressure, by varying two design parameters at the time, for the most relevant combinations, while

maintaining the others fixed at the nominal value, for the “healthy”, “diseased I”, and “diseased II” aortic root configurations

cycle time and costs. Within this context, the present work proposes a computational framework for the shape and cross-sectional size optimization of TAV frames based on FE analysis of TAV implantation in idealized aortic root models.

Several approaches have been proposed where computer models were applied to endovascular devices shape optimization. While the majority of these works were focused on coronary and peripheral stents (Li et al. 2009, 2013; Wu et al. 2010; Pant et al. 2011, 2012; Azaouzi et al. 2013; Li and Wang 2013; Clune et al. 2014; Tammareddi et al. 2016; Alaimo et al. 2017), little attention has been paid to TAVs until now.

#### 4.1 Technical characteristics and novelty items of the proposed optimization framework

In a recent study, TAV shape optimization was focused on the inflow portion of the valve frame, considering two specific geometrical parameters of that region, i.e., the valve diameter at 4 mm above the ventricular inflow section and the height of the first row of the frame cells at the ventricular inflow (Rocatello et al. 2019). In contrast, here, six parameters associated with the overall TAV frame geometry were considered for design optimization purposes, thus providing a comprehensive picture of the overall impact of frame geometric

**Table 5** Objectives values for the nominal and optimized geometries

Aortic root	Healthy		Diseased I			Diseased II		
	Nom.	Opt. 1	Nom.	Opt. 2	Opt. 4	Nom.	Opt. 3	Opt. 4
Pullout force magnitude (N)	2.33	5.53	16.92	11.37	20.70	19.49	16.59	25.67
Peak maximum principal stress (MPa)	0.56	0.94	1.91	0.81	1.66	1.70	1.48	1.59
Peak maximum contact pressure (MPa)	0.66	0.50	0.56	0.21	0.33	0.00	0.22	0.09

Opt. 1 optimized 1, Opt. 2 optimized 2, Opt. 2 optimized 2, Opt. 3 optimized 3, Opt. 4 optimized 4

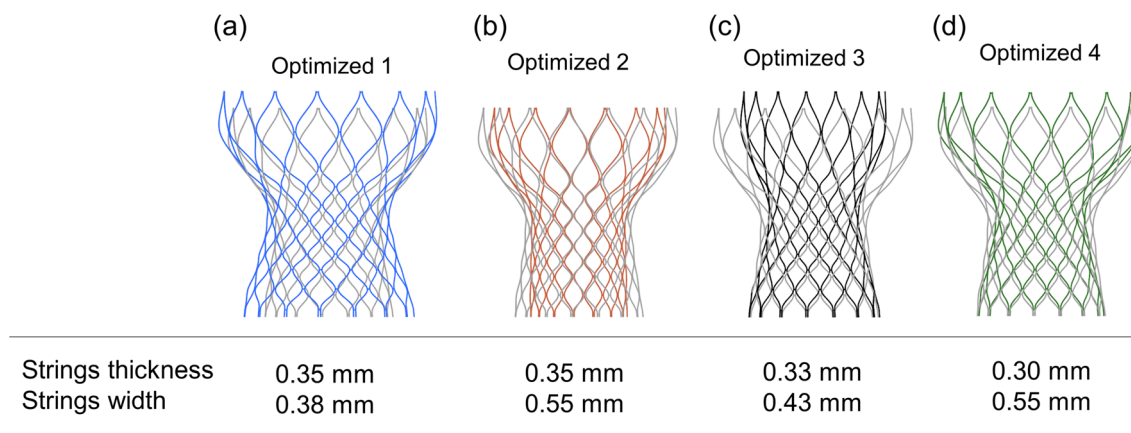


**Fig. 10** Optimized TAV frame geometries, overlapped to the nominal geometry (in gray), and the corresponding string cross-section values for the **a** “healthy” (“optimized 1”), **b** “diseased I” (“optimized 2”), and

**c** “diseased II” (“optimized 3”) configurations, and for **d** both “diseased” configurations simultaneously (“optimized 4”)

attributes on TAV implantation procedural effectiveness. Furthermore, as a novelty of this study, here the implicit FE analysis was implemented in the optimization framework, taking advantage of its being unconditionally stable, not requiring small time step size and mass scaling to guarantee an accurate and stable solution.

To perform the number of simulations required by the proposed optimization framework ( $n = 77$  for each aortic root configuration), a computationally efficient FE model of TAV implantation was defined adopting 1D and 2D elements for the TAV frame and the aortic root and proper model simplifications in addition to the implicit FE solver. The run time of each sample simulation was  $\sim 40$ ,  $\sim 75$ , and  $\sim 80$  min on 6 computing cores of a local workstation, depending on the healthy, diseased I, and diseased II aortic root configuration, respectively. Ideally, all simulations required by the central composite design sampling strategy could be simultaneously performed on a large computing cluster, obtaining the optimization results in less than 2 h. Computational efficiency was also demonstrated when comparing the run time to the

previous TAV frame optimization study (Rocatello et al. 2019), where the average run time for each sample simulation was 53 min on a cluster equipped with 16 computing cores (4.0 GHz and 63.0 GB RAM for each node).

#### 4.2 Consistency check of the optimization framework

The simulations of the impact of TAV implantation satisfactorily agreed in terms of optimization objectives with data reported by the literature. In particular, a marked dependency of the results with respect to the presence of calcium deposits was observed, according to previous findings (Sturla et al. 2016). The observed dependence of the obtained pullout force magnitude values on the aortic configuration agreed with previous findings (Wang et al. 2012, 2015) reporting values considerably higher in diseased aortic root configurations, as compared to the healthy one (Table 5). The here observed high pullout force magnitude values in the presence of calcium deposits were ascribable to the combined effect of the adopted value of friction coefficient between the TAV frame

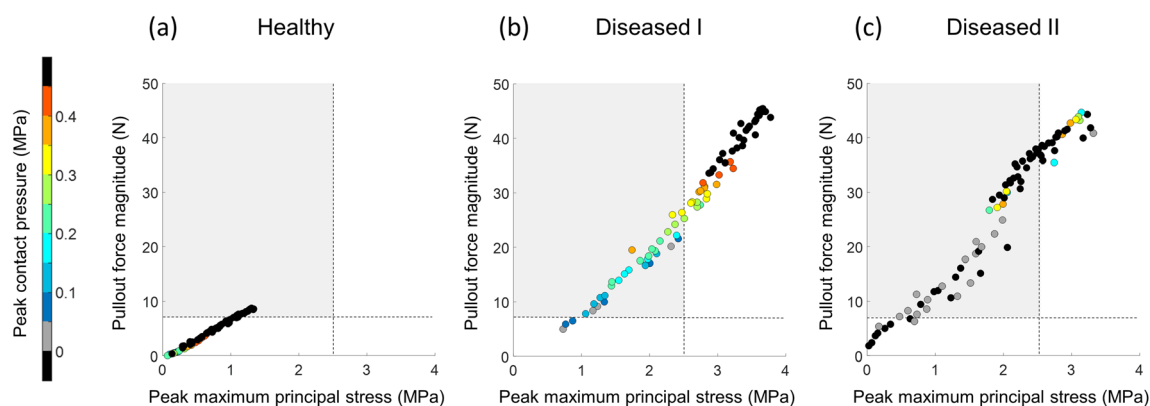
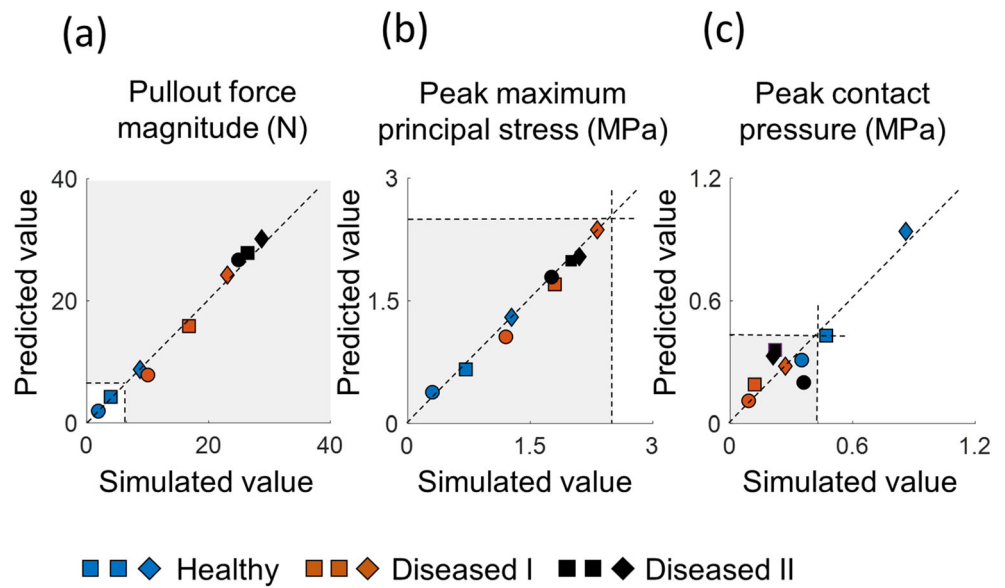


**Fig. 11** Pareto-optimal solutions of the three objectives for the **a** “healthy”, **b** “diseased I”, and **c** “diseased II” aortic root configurations. Points were represented in the plane of pullout force magnitude vs. peak maximum principal stress and were colored according to the values of

peak contact pressure. Feasible values of pullout force magnitude and peak maximum principal stress were identified within a transparent gray region. Constraints of the objectives are indicated as a dotted line, illustrating the feasible solution space as a transparent gray region

**Fig. 12** Predicted values of **a** pullout force magnitude, **b** peak maximum principal stress, and **c** peak contact pressure, in function of the corresponding simulated values, for three Pareto-optimal solutions of each aortic root configuration (i.e., “healthy”, “diseased I”, and “diseased II” configuration). Constraints of the objectives are indicated as a dotted line, illustrating the feasible solution space as a transparent gray region



and the calcium deposits, and to the normal contact forces related to the reduced TAV frame expansion (Fig. 5a). Indeed, previous studies suggested that calcium deposits help the TAV frame anchoring (McGee et al. 2019b) and that additional oversizing of the device should be accounted for to avoid migration issues in the absence of calcifications (Mummert et al. 2013). In addition, the observed peak maximum principal stress values were higher in the case of diseased configurations as compared to the healthy one (Table 5). The explanation for this lies in the presence of calcium deposits, pushed by the TAV frame against the aortic root wall (Fig. 5b). Moreover, peak maximum principal stress values depended both on calcium deposit shape and position. Overall, the reported peak maximum principal stress values were similar to those reported in previous FE studies of TAV implantation (Morganti et al. 2014; Wang et al. 2015; McGee et al. 2019a). Peak contact pressure values in the diseased configurations were lower than those in the healthy one (Table 5, Fig. 5c). This was attributable to a dependence on the calcium pattern, as well as to the fact that contact forces were mainly exerted between TAV frame and calcium deposits, instead of the aortic root wall (Fig. 5a). Indeed, the zero peak contact pressure reported for the diseased II configuration was related to the absence of contact between the TAV frame and the LVOT (Fig. 5c), indicating the possible occurrence of PVL.

### 4.3 Analysis of surrogate models

After a preliminary analysis that compared the coupling of different sampling strategies and surrogate models (see [Supplementary Materials](#)), the combination of central composite design with Gauss process surrogate model was successfully used, enabling the definition of an approximate relationship

between the optimization objectives and the TAV design parameters. In this regard, a first analysis conducted by varying two design parameters at a time while maintaining the others fixed at the nominal value (Fig. 9) allowed to clarify the impact of the design parameters on the predicted objective values and, consequently, to make decisions on the TAV frame design based on the predicted mechanical behavior. However, this approach involved a limited search of the design space and parameter exploration. Hence, all parameter combinations within the design space were also investigated using two alternative approaches to identify optimal candidates starting from the nominal geometry of the TAV frame, namely (1) a conservative constraint-based approach and (2) an approach based on Pareto optimality. The two approaches were applied to all the aortic root configurations. In particular, the healthy configuration was included into the analysis as it represents the extreme configuration without calcification, useful in the prospective that TAV replacement could become an important treatment option also for low-risk patients (Howard et al. 2019), presenting with very low calcium deposits volume. The conservative constraint-based approach successfully led to one optimized TAV frame shape for each specific aortic root configuration (i.e., optimized I, II, and III geometries) and one optimized shape for both diseased configurations (i.e., optimized IV geometry) (Table 5, Fig. 10). Based on this approach, no feasible solution emerged for the healthy configuration (Table 5), suggesting the occurrence of possible prosthesis-patient mismatch in the absence of calcifications and indicating the need to further extend the initial design space to account for additional device oversizing. Conversely, the other optimized geometries based on diseased configurations were identified within the feasible solution space (Table 5), revealing the ability of our approach to obtain optimal candidates within the design space, fitted to specific or grouped diseased anatomies. The approach based on Pareto optimality led to a set of optimal TAV

frame geometry candidates for each aortic root configuration (Fig. 11). Thereafter, design candidates could be selected based on additional features related to, e.g., hemodynamics, manufacturing-related aspects, the interface with the sutured prosthetic valve and costs, ultimately ensuring high flexibility over the device design process.

#### 4.4 Limitations and future perspectives

This study presents some limitations that might weaken the effectiveness of the proposed optimization procedure. Idealized FE models of the aortic root were considered. In particular, the heterogeneous composition and thickness of the arterial wall and native leaflets was neglected. The shape of the calcium deposits was assumed as an arc shape structure with a homogenous, isotropic material. Moreover, further investigations could be conducted to improve the efficiency and robustness of the optimization process in terms of computational time and accuracy (Giselle Fernández-Godino et al. 2019), evaluating the use of more advanced optimization algorithms. Despite the limitations, the optimization framework proved to be effective in identifying appropriate TAV frame shapes and several advances could be implemented to further extend its potential. In detail, aortic root models with different dimension/shape could be investigated to derive an optimized TAV frame geometry suitable for a range of anatomical sizes. Other anatomical features, such as the aortic root eccentricity or different calcification patterns, could be analyzed. Furthermore, the optimization framework could be used to improve other aspects related to the TAV mechanical performance such as the Nitinol material parameters, string thickness distribution, and device implantation positioning. Different TAV frame designs could be investigated as well. Finally, FE simulations could be coupled with computation fluid dynamics simulations, following device implantation, in order to address TAV implantation procedural complications such as PVL (De Jaegere et al. 2016; Mao et al. 2018; Rocatello et al. 2019) and thrombosis (Bianchi et al. 2019; Nappi et al. 2020).

## 5 Conclusions

In this work, a computational framework for the shape and cross-sectional size optimization of TAV frames was proposed. FE analyses of TAV deployment were performed in three idealized different aortic root models representing a healthy (i.e., without calcium) and two diseased (i.e., with calcium deposits) scenarios. Three biomechanical quantities (i.e., pullout force magnitude, peak maximum principal stress within the aortic wall, and peak contact pressure in the LVOT) were defined as objectives of the optimization problem to evaluate the TAV frame mechanical performance. By

defining a fixed design space and implementing surrogate models related to the optimization objectives, the geometrical parameters of the TAV frame were explored to improve its mechanical performance. Thereafter, optimized frame geometries were successfully identified, for both single and groups of anatomies, ultimately resulting in improved procedural outcomes and reduced time and costs associated with the device iterative development cycle. The optimization framework provided enough flexibility to be extended on further studies accounting for different aortic root anatomies, additional design parameters, and other TAV devices.

**Supplementary Information** The online version contains supplementary material available at <https://doi.org/10.1007/s00158-021-02944-w>.

**Authors' contributions** Conceptualization: D.C., U.M., A.A., C.C.; Data curation: D.C.; Simulations: D.C.; Post-processing of the results: D.C.; Interpretation of data: D.C., D.G., U.M., A.A., C.C.; Supervision: C.C., U.M., A.A.; Writing—original draft preparation: D.C., C.C.; Writing—review and editing: D.C., D.G., U.M., A.A. C.C. All authors discussed the results and reviewed the manuscript.

**Funding** Open access funding provided by Politecnico di Torino within the CRUI-CARE Agreement. This work has been supported by the Italian Ministry of Education, University and Research (FISR2019\_03221, CECOMES) and by the Piedmont Region, Italy (POR FESR PiTeF 2014-20 351-96, Nitoliera).

**Code availability** Commercial software (i.e., Matlab, HyperMesh, and Abaqus) were used to perform all FE analyses and post-process the results.

#### Declarations

**Conflict of interest** The authors declare that they have no conflict of interest.

**Replication of results** The necessary information for replication of the results, including the geometric, material, and meshing data of the models, and the simulation settings, is presented in this paper. The interested reader may contact the corresponding author for further implementation details.

**Open Access** This article is licensed under a Creative Commons Attribution 4.0 International License, which permits use, sharing, adaptation, distribution and reproduction in any medium or format, as long as you give appropriate credit to the original author(s) and the source, provide a link to the Creative Commons licence, and indicate if changes were made. The images or other third party material in this article are included in the article's Creative Commons licence, unless indicated otherwise in a credit line to the material. If material is not included in the article's Creative Commons licence and your intended use is not permitted by statutory regulation or exceeds the permitted use, you will need to obtain permission directly from the copyright holder. To view a copy of this licence, visit <http://creativecommons.org/licenses/by/4.0/>.

## References

- Abaqus (2016). Abaqus 2016 analysis user's guide. Dassault Systemes, Simulia
- Alaimo G, Auricchio F, Conti M, Zingales M (2017) Multi-objective optimization of nitinol stent design. *Med Eng Phys* 47:13–24. <https://doi.org/10.1016/j.medengphy.2017.06.026>
- Auricchio F, Conti M, Morganti S, Reali A (2014) Simulation of transcatheter aortic valve implantation: a patient-specific finite element approach. *Comput Methods Biomech Biomed Eng* 17:1347–1357. <https://doi.org/10.1080/10255842.2012.746676>
- Auricchio F, Conti M, Morganti S, Totaro P (2011) A computational tool to support pre-operative planning of stentless aortic valve implant. *Med Eng Phys* 33:1183–1192. <https://doi.org/10.1016/j.medengphy.2011.05.006>
- Auricchio F, Taylor RL (1997) Shape-memory alloys: modelling and numerical simulations of the finite-strain superelastic behavior. *Comput Methods Appl Mech Eng* 143:175–194. [https://doi.org/10.1016/S0045-7825\(96\)01147-4](https://doi.org/10.1016/S0045-7825(96)01147-4)
- Azaouzi M, Makradi A, Belouettar S (2013) Numerical investigations of the structural behavior of a balloon expandable stent design using finite element method. *Comput Mater Sci* 72:54–61. <https://doi.org/10.1016/j.commatsci.2013.01.031>
- Bailey J, Curzen N, Bressloff NW (2016) Assessing the impact of including leaflets in the simulation of TAVI deployment into a patient-specific aortic root. *Comput Methods Biomech Biomed Eng* 19:733–744. <https://doi.org/10.1080/10255842.2015.1058928>
- Bianchi M, Marom G, Ghosh RP et al (2019) Patient-specific simulation of transcatheter aortic valve replacement: impact of deployment options on paravalvular leakage. *Biomech Model Mechanobiol* 18:435–451. <https://doi.org/10.1007/s10237-018-1094-8>
- Bosi GM, Capelli C, Cheang MH et al (2018) Population-specific material properties of the implantation site for transcatheter aortic valve replacement finite element simulations. *J Biomech* 71:236–244. <https://doi.org/10.1016/j.jbiomech.2018.02.017>
- Bressloff NW, Ragkousis G, Curzen N (2016) Design optimisation of coronary artery stent systems. *Ann Biomed Eng* 44:357–367. <https://doi.org/10.1007/s10439-015-1373-9>
- Cabrera MS, Oomens CWJ, Baaijens FPT (2017) Understanding the requirements of self-expandable stents for heart valve replacement: radial force, hoop force and equilibrium. *J Mech Behav Biomed Mater* 68:252–264. <https://doi.org/10.1016/j.jmbbm.2017.02.006>
- Clune R, Kelliher D, Robinson JC, Campbell JS (2014) NURBS modeling and structural shape optimization of cardiovascular stents. *Struct Multidiscip Optim* 50:159–168. <https://doi.org/10.1007/s00158-013-1038-y>
- Dasi LP, Hatoum H, Kheradvar A et al (2017) On the mechanics of transcatheter aortic valve replacement. *Ann Biomed Eng* 45:310–331. <https://doi.org/10.1007/s10439-016-1759-3>
- De Biase C, Mastrokostopoulos A, Philippart R et al (2018) What are the remaining limitations of TAVI? *J Cardiovasc Surg* 59:373–380. <https://doi.org/10.23736/s0021-9509.18.10489-7>
- De Jaegere P, De Santis G, Rodriguez-Olivares R et al (2016) Patient-specific computer modeling to predict aortic regurgitation after transcatheter aortic valve replacement. *JACC Cardiovasc Interv* 9:508–512. <https://doi.org/10.1016/j.jcin.2016.01.003>
- Deb K, Pratap A, Agarwal S, Meyarivan T (2002) A fast and elitist multiobjective genetic algorithm: NSGA-II. *IEEE Trans Evol Comput* 6:182–197. <https://doi.org/10.1109/4235.996017>
- Draper NR, Lin DKJ (1996) Response surface designs. In: North-Holland (ed) *Handbook of statistics*. pp 343–375
- Durko AP, Osnabrugge RL, Van Mieghem NM et al (2018) Annual number of candidates for transcatheter aortic valve implantation per country: current estimates and future projections. *Eur Heart J* 39:2635–2642. <https://doi.org/10.1093/eurheartj/ehy107>
- Fanning JP, Platts DG, Walters DL, Fraser JF (2013) Transcatheter aortic valve implantation (TAVI): valve design and evolution. *Int J Cardiol* 168:1822–1831. <https://doi.org/10.1016/j.ijcard.2013.07.117>
- Finotello A, Morganti S, Auricchio F (2017) Finite element analysis of TAVI: impact of native aortic root computational modeling strategies on simulation outcomes. *Med Eng Phys* 47:2–12. <https://doi.org/10.1016/j.medengphy.2017.06.045>
- Formato GM, Lo Rito M, Auricchio F et al (2018) Aortic expansion induces lumen narrowing in anomalous coronary arteries: a parametric structural finite element analysis. *J Biomech Eng* 140:1–9. <https://doi.org/10.1115/1.4040941>
- Gessat M, Hopf R, Pollok T et al (2014) Image-based mechanical analysis of stent deformation: concept and exemplary implementation for aortic valve stents. *IEEE Trans Biomed Eng* 61:4–15. <https://doi.org/10.1109/TBME.2013.2273496>
- Giselle Fernández-Godino M, Park C, Kim NH, Haftka RT (2019) Issues in deciding whether to use multifidelity surrogates. *AIAA J* 57:2039–2054. <https://doi.org/10.2514/1.J057750>
- Gunning PS, Vaughan TJ, McNamara LM (2014) Simulation of self expanding transcatheter aortic valve in a realistic aortic root: implications of deployment geometry on leaflet deformation. *Ann Biomed Eng* 42:1989–2001. <https://doi.org/10.1007/s10439-014-1051-3>
- Hall GJ, Kasper EP (2006) Comparison of element technologies for modeling stent expansion. *J Biomech Eng* 128:751–756. <https://doi.org/10.1115/1.2264382>
- Hopf R, Gessat M, Russ C et al (2017) Finite element stent modeling for the postoperative analysis of transcatheter aortic valve implantation. *J Med Devices, Trans ASME* 11:1–7. <https://doi.org/10.1115/1.4036334>
- Howard C, Jullian L, Joshi M et al (2019) TAVI and the future of aortic valve replacement. *J Card Surg* 34:1577–1590. <https://doi.org/10.1111/jocs.14226>
- Jones BM, Krishnaswamy A, Tuzcu EM et al (2017) Matching patients with the ever-expanding range of TAVI devices. *Nat Rev Cardiol* 14:615–626. <https://doi.org/10.1038/nrcardio.2017.82>
- Jones DR, Schonlau M, Welch WJ (1998) Efficient global optimization of expensive black-box functions. *J Glob Optim* 13:455–492. <https://doi.org/10.1023/A:1008306431147>
- Labrosse MR, Beller CJ, Robicsek F, Thubrikar MJ (2006) Geometric modeling of functional trileaflet aortic valves: development and clinical applications. *J Biomech* 39:2665–2672. <https://doi.org/10.1016/j.jbiomech.2005.08.012>
- Li H, Qiu T, Zhu B et al (2013) Design optimization of coronary stent based on finite element models. *Sci World J* 2013:630243. <https://doi.org/10.1155/2013/630243>
- Li H, Wang X (2013) Design optimization of balloon-expandable coronary stent. *Struct Multidiscip Optim* 48:837–847. <https://doi.org/10.1007/s00158-013-0926-5>
- Li N, Zhang H, Ouyang H (2009) Shape optimization of coronary artery stent based on a parametric model. *Finite Elem Anal Des* 45:468–475. <https://doi.org/10.1016/j.finel.2009.01.001>
- Luraghi G, Matas JFR, Beretta M et al (2020) The impact of calcification patterns in transcatheter aortic valve performance: a fluid-structure interaction analysis. *Comput Methods Biomech Biomed Eng*. in press. <https://doi.org/10.1080/10255842.2020.1817409>
- Luraghi G, Rodriguez Matas JF, Migliavacca F (2021) In silico approaches for transcatheter aortic valve replacement inspection. *Expert Rev Cardiovasc Ther* 19:61–70. <https://doi.org/10.1080/14779072.2021.1850265>
- Mao W, Wang Q, Kodali S, Sun W (2018) Numerical parametric study of paravalvular leak following a transcatheter aortic valve deployment into a patient-specific aortic root. *J Biomech Eng* 140:1–11. <https://doi.org/10.1115/1.4040457>
- McGee OM, Gunning PS, McNamara A, McNamara LM (2019a) The impact of implantation depth of the Lotus™ valve on mechanical

- stress in close proximity to the bundle of His. *Biomech Model Mechanobiol* 18:79–88. <https://doi.org/10.1007/s10237-018-1069-9>
- McGee OM, Sun W, McNamara LM (2019b) An in vitro model quantifying the effect of calcification on the tissue–stent interaction in a stenosed aortic root. *J Biomech* 82:109–115. <https://doi.org/10.1016/j.jbiomech.2018.10.010>
- McKay MD, Beckman RJ, Conover WJ (1979) Comparison of three methods for selecting values of input variables in the analysis of output from a computer code. *Technometrics* 21:239–245. <https://doi.org/10.1080/00401706.1979.10489755>
- Medtronic (2014) Instruction for use, CoreValve system. Transcatheter aortic valve, delivery catheter system, compression loading system. Medtronic
- Morganti S, Brambilla N, Petronio AS et al (2016) Prediction of patient-specific post-operative outcomes of TAVI procedure: the impact of the positioning strategy on valve performance. *J Biomech* 49:2513–2519. <https://doi.org/10.1016/j.jbiomech.2015.10.048>
- Morganti S, Conti M, Aiello M et al (2014) Simulation of transcatheter aortic valve implantation through patient-specific finite element analysis: two clinical cases. *J Biomech* 47:2547–2555. <https://doi.org/10.1016/j.jbiomech.2014.06.007>
- Morrison TM, Dreher ML, Nagaraja S et al (2017) The role of computational modeling and simulation in the total product life cycle of peripheral vascular devices. *J Med Devices, Trans ASME* 11:1–10. <https://doi.org/10.1115/1.4035866>
- Morrison TM, Pathmanathan P, Adwan M, Margerrison E (2018) Advancing regulatory science with computational modeling for medical devices at the FDA’s office of science and engineering laboratories. *Front Med* 5:1–11. <https://doi.org/10.3389/fmed.2018.00241>
- Mummert J, Sirois E, Sun W (2013) Quantification of biomechanical interaction of transcatheter aortic valve stent deployed in porcine and ovine hearts. *Ann Biomed Eng* 41:577–586. <https://doi.org/10.1007/s10439-012-0694-1>
- Nappi F, Mazzocchi L, Timofeva I et al (2020) A finite element analysis study from 3D CT to predict transcatheter heart valve thrombosis. *Diagnostics* 10:183. <https://doi.org/10.3390/diagnostics10040183>
- Neragi-Miandoab S, Michler RE (2013) A review of most relevant complications of transcatheter aortic valve implantation. *ISRN Cardiol* 2013:956252. <https://doi.org/10.1155/2013/956252>
- Ovcharenko EA, Klyshnikov KU, Yuzhalin AE et al (2016) Modeling of transcatheter aortic valve replacement: patient specific vs general approaches based on finite element analysis. *Comput Biol Med* 69:29–36. <https://doi.org/10.1016/j.combiomed.2015.12.001>
- Pant S, Bressloff NW, Limbert G (2012) Geometry parameterization and multidisciplinary constrained optimization of coronary stents. *Biomech Model Mechanobiol* 11:61–82. <https://doi.org/10.1007/s10237-011-0293-3>
- Pant S, Limbert G, Curzen NP, Bressloff NW (2011) Multiobjective design optimisation of coronary stents. *Biomaterials* 32:7755–7773. <https://doi.org/10.1016/j.biomaterials.2011.07.059>
- Pawade T, Clavel MA, Tribouilloy C et al (2018) Computed tomography aortic valve calcium scoring in patients with aortic stenosis. *Circ Cardiovasc Imaging* 11:1–11. <https://doi.org/10.1161/CIRCIMAGING.117.007146>
- Rasmussen CE, Williams CKI (2018) Gaussian processes for machine learning. The MIT Press
- Rocatello G, De Santis G, De Bock S et al (2019) Optimization of a transcatheter heart valve frame using patient-specific computer simulation. *Cardiovasc Eng Technol* 10:456–468. <https://doi.org/10.1007/s13239-019-00420-7>
- Rocatello G, El Faquir N, De Santis G et al (2018) Patient-specific computer simulation to elucidate the role of contact pressure in the development of new conduction abnormalities after catheter-based implantation of a self-expanding aortic valve. *Circ Cardiovasc Interv* 11:1–9. <https://doi.org/10.1161/CIRCINTERVENTIONS.117.005344>
- Rotman OM, Bianchi M, Ghosh RP et al (2018) Principles of TAVR valve design, modelling, and testing. *Expert Rev Med Devices* 15: 771–791. <https://doi.org/10.1080/17434440.2018.1536427>
- Schultz C, Rodriguez-Olivares R, Bosmans J et al (2016) Patient-specific image-based computer simulation for the prediction of valve morphology and calcium displacement after TAVI with the Medtronic CoreValve and the Edwards SAPIEN valve. *EuroIntervention* 11: 1044–1052. <https://doi.org/10.4244/EIJV11I9A212>
- Sturla F, Ronzoni M, Vitali M et al (2016) Impact of different aortic valve calcification patterns on the outcome of transcatheter aortic valve implantation: a finite element study. *J Biomech* 49:2520–2530. <https://doi.org/10.1016/j.jbiomech.2016.03.036>
- Tabata N, Sinning JM, Kaikita K et al (2019) Current status and future perspective of structural heart disease intervention. *J Cardiol* 74:1–12. <https://doi.org/10.1016/j.jcc.2019.02.022>
- Tammareddi S, Sun G, Li Q (2016) Multiobjective robust optimization of coronary stents. *Mater Des* 90:682–692. <https://doi.org/10.1016/j.matdes.2015.10.153>
- Tanaka Y, Saito S, Sasuga S et al (2018) Quantitative assessment of paravalvular leakage after transcatheter aortic valve replacement using a patient-specific pulsatile flow model. *Int J Cardiol* 258: 313–320. <https://doi.org/10.1016/j.ijcard.2017.11.106>
- Thubrikar MJ, Aouad J, Nolan SP (1986) Patterns of calcific deposits in operatively excised stenotic or purely regurgitant aortic valves and their relation to mechanical stress. *Am J Cardiol* 58:304–308. [https://doi.org/10.1016/0002-9149\(86\)90067-6](https://doi.org/10.1016/0002-9149(86)90067-6)
- Tzamtzis S, Viquerat J, Yap J et al (2013) Numerical analysis of the radial force produced by the Medtronic-CoreValve and Edwards-SAPIEN after transcatheter aortic valve implantation (TAVI). *Med Eng Phys* 35:125–130. <https://doi.org/10.1016/j.medengphy.2012.04.009>
- Wang Q, Kodali S, Primiano C, Sun W (2015) Simulations of transcatheter aortic valve implantation: implications for aortic root rupture. *Biomech Model Mechanobiol* 14:29–38. <https://doi.org/10.1007/s10237-014-0583-7>
- Wang Q, Sirois E, Sun W (2012) Patient-specific modeling of biomechanical interaction in transcatheter aortic valve deployment. *J Biomech* 45:1965–1971. <https://doi.org/10.1016/j.jbiomech.2012.05.008>
- Wu W, Petrini L, Gastaldi D et al (2010) Finite element shape optimization for biodegradable magnesium alloy stents. *Ann Biomed Eng* 38:2829–2840. <https://doi.org/10.1007/s10439-010-0057-8>
- Yusoff Y, Ngadiman MS, Zain AM (2011) Overview of NSGA-II for optimizing machining process parameters. *Procedia Eng* 15:3978–3983. <https://doi.org/10.1016/j.proeng.2011.08.745>

**Publisher's note** Springer Nature remains neutral with regard to jurisdictional claims in published maps and institutional affiliations.